

---

# AN UPPER BOUND FOR THE DISTRIBUTION OVERLAP INDEX AND ITS APPLICATIONS

**Hao Fu**

hf881@nyu.edu

Department of Electrical and Computer Engineering,  
New York University, Brooklyn, NY 11201, USA

**Prashanth Krishnamurthy**

krishnamurthy.prashanth@nyu.edu

Department of Electrical and Computer Engineering,  
New York University, Brooklyn, NY 11201, USA

**Siddharth Garg**

sg175@nyu.edu

Department of Electrical and Computer Engineering,  
New York University, Brooklyn, NY 11201, USA

**Farshad Khorrami**

khorrami@nyu.edu

Department of Electrical and Computer Engineering  
New York University, Brooklyn, NY 11201, USA

## ABSTRACT

This paper proposes an easy-to-compute upper bound for the overlap index between two probability distributions without requiring any knowledge of the distribution models. The computation of our bound is time-efficient and memory-efficient and only requires finite samples. The proposed bound shows its value in one-class classification and domain shift analysis. Specifically, in one-class classification, we build a novel one-class classifier by converting the bound into a confidence score function. Unlike most one-class classifiers, the training process is not needed for our classifier. Additionally, the experimental results show that our classifier can be accurate with only a small number of in-class samples and outperforms many state-of-the-art methods on various datasets in different one-class classification scenarios. In domain shift analysis, we propose a theorem based on our bound. The theorem is useful in detecting the existence of domain shift and inferring data information. The detection and inference processes are both computation-efficient and memory-efficient. Our work shows significant promise toward broadening the applications of overlap-based metrics.

## 1 INTRODUCTION

Measuring the similarity between distributions is a popular topic in the machine learning study. However, compared to other metrics that measure the distribution similarity, the literature on the distribution overlap index is thin. This paper contributes to the study of the overlap index which is defined as the area intersected by two probability density functions shown in Fig. 1(a). Specifically, unlike most related works that have strong distribution assumptions (e.g., symmetry or unimodality), this work proposes an upper bound for the overlap index with distribution-free settings, in which the probability distributions are unknown. The bound is easy to compute and contains two key terms: the norm of the difference between the two distributions' means and a variation distance between the two distributions over a subset. The computation of the bound is time-efficient and memory-efficient and requires only finite samples. Even though finding such an upper bound for the distribution overlap index is already valuable, we further explore two additional applications of our bound as discussed below to broaden the applications of overlap-based metrics.

One application of our bound is for one-class classification. Specifically, one-class classification refers to a model that outputs positive for in-class samples and negative for out-class samples that are absent, poorly sampled, or not well defined (i.e., Fig. 1(b)). We proposed a novel one-class classifier by converting our bound into a confidence score function to evaluate if a sample is in-class or out-class. The proposed classifier has many advantages. For example, implementing deep neural network-based classifiers requires training thousands of parameters and large memory, whereas implementing our classifier does not require the training process. It only needs sample norms to calculate the confidence score. Besides, deep neural network-based classifiers need rela-

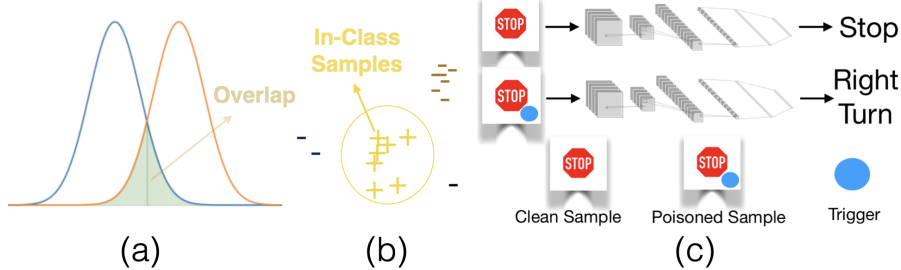


Figure 1: (a): Overlap of two distributions. (b): One-class classification. (c): Backdoor attack.

tively large amounts of data to avoid under-fitting or over-fitting, whereas our method is empirically accurate with only a small number of in-class samples. Therefore, our classifier is computation-efficient, memory-efficient, and data-efficient. Additionally, compared with other traditional one-class classifiers, such as Gaussian distribution-based classifier, Mahalanobis distance-based classifier (Lee et al., 2018) and one-class support vector machine (Schölkopf et al., 2001), our classifier is distribution-free, explainable, and easy to understand. The experimental results show that the proposed one-class classifier outperforms many state-of-the-art methods on various datasets in different one-class classification scenarios.

Another application of our bound is for domain shift analysis. Specifically, a domain shift is a change in the dataset distribution between a model’s training dataset and the testing dataset encountered during implementation (i.e., the overlap index value between the distributions of the two datasets is less than 1). We proposed a theorem to calculate the model’s testing accuracy in terms of the overlap index between the distributions of the training and testing datasets and further found the upper limit of the accuracy using our bound for the overlap index. The theorem is useful in detecting the existence of domain shift and inferring data information. Additionally, the detection and inference processes using the proposed theorem are both computation-efficient and memory-efficient and do not require the training process.

Overall, the contributions of this paper include:

- Deriving a distribution-free upper bound for the overlap index.
- Building a novel one-class classifier with the bound being the confidence score function.
- Showing the outperformance of the one-class classifier over various state-of-the-art methods on several datasets, including UCI datasets, CIFAR-100, sub-ImageNet, etc., and in different one-class classification scenarios, such as novelty detection, anomaly detection, out-of-distribution detection, and neural network backdoor detection.
- Proposing a theorem based on the derived bound to detect the existence of domain shift and infer useful data information.

### 1.1 BACKGROUND AND RELATED WORKS

**Measuring the similarity between distributions:** Gini & Livada (1943) and Weitzman (1970) introduced the concept of the distribution overlap index. Other measurements for the similarity between distributions include the total variation distance, Kullback-Leibler divergence (Kullback & Leibler, 1951), Bhattacharyya’s distance (Bhattacharyya, 1943), and Hellinger distance (Hellinger, 1909). In psychology, some effect size measures’ definitions involve the concept of the distribution overlap index, such as Cohen’s U index (Cohen, 2013), McGraw and Wong’s CL measure (McGraw & Wong, 1992), and Huberty’s I degree of non-overlap index (Huberty & Lowman, 2000). However, they all have strong distribution assumptions (e.g., symmetry or unimodality) regarding the overlap index. Pastore & Calcagnì (2019) approximates the overlap index via kernel density estimators.

**One-class classification:** Moya & Hush (1996) coined the term one-class classification. One-class classification intersects with novelty detection, anomaly detection, out-of-distribution detection, and outlier detection. Yang et al. (2021) explains the differences among these detection areas. Khan & Madden (2014) discusses many traditional non neural network-based one-class classifiers, such as

---

one-class support vector machine (Schölkopf et al., 2001), decision-tree (Comité et al., 1999), and one-class nearest neighbor (Tax, 2002). Two neural network-based one-class classifiers are (Ruff et al., 2018) and OCGAN (Perera et al., 2019). Morteza & Li (2022) introduces a Gaussian mixture-based energy measurement and compares it with several other score functions, including maximum softmax score (Hendrycks & Gimpel, 2017), maximum Mahalanobis distance (Lee et al., 2018), and energy score (Liu et al., 2020a) for one-class classification.

**Neural network backdoor attack and detection:** Gu et al. (2019) and Liu et al. (2018b) mentioned the concept of the neural network backdoor attack. The attack contains two steps: during training, the attacker injects triggers into the training dataset; during testing, the attacker leads the network to misclassify by presenting the triggers (i.e., Fig. 1(c)). The data poisoning attack (Biggio et al., 2012) and adversarial attack (Goodfellow et al., 2014) overlap with the backdoor attack. Some proposed trigger types are Wanet (Nguyen & Tran, 2021), invisible sample-specific (Li et al., 2021), smooth (Zeng et al., 2021), and reflection (Liu et al., 2020b). Some methods protecting neural networks from backdoor attacks include neural cleanse (Wang et al., 2019), fine-pruning (Liu et al., 2018a), and STRIP (Gao et al., 2019). NNoculation (Veldanda et al., 2021) and RAID (Fu et al., 2022) utilize online samples to improve their detection methods. The backdoor detection problem also intersects with one-class classification. Therefore, some one-class classifiers can detect poisoned samples against the neural network backdoor attack.

**Organization of the Paper:** We first provide preliminaries and derive the proposed upper bound for the overlap index in Sec. 2. We next apply our bound to domain shift analysis in Sec. 4. We then propose, analyze, and evaluate our novel one-class classifier in Sec. 3. We finally conclude the paper in Section 5.

## 2 AN UPPER BOUND FOR THE OVERLAP INDEX

### 2.1 PRELIMINARIES

For simplicity, we consider the  $\mathbb{R}^n$  space and continuous random variables. We also define  $P$  and  $Q$  as two probability distributions in  $\mathbb{R}^n$  with  $f_P$  and  $f_Q$  being their probability density functions.

**Definition 1** (Overlap Index). *The overlap  $\eta : \mathbb{R}^n \times \mathbb{R}^n \rightarrow [0, 1]$  of the two distributions is defined:*

$$\eta(P, Q) = \int_{\mathbb{R}^n} \min[f_P(x), f_Q(x)] dx. \quad (1)$$

**Definition 2** (Total Variation Distance). *The total variation distance  $\delta : \mathbb{R}^n \times \mathbb{R}^n \rightarrow [0, 1]$  of the two distributions is defined as*

$$\delta(P, Q) = \frac{1}{2} \int_{\mathbb{R}^n} |f_P(x) - f_Q(x)| dx. \quad (2)$$

**Definition 3** (Variation Distance on Subsets). *Given a subset  $A$  from  $\mathbb{R}^n$ , we define  $\delta_A : \mathbb{R}^n \times \mathbb{R}^n \rightarrow [0, 1]$  to be the variation distance of the two distributions on  $A$ , which is*

$$\delta_A(P, Q) = \frac{1}{2} \int_A |f_P(x) - f_Q(x)| dx. \quad (3)$$

**Remark 1.** *One can prove that  $\eta$  and  $\delta$  satisfy the following equation:*

$$\eta(P, Q) = 1 - \delta(P, Q) = 1 - \delta_A(P, Q) - \delta_{\mathbb{R}^n \setminus A}(P, Q). \quad (4)$$

*The quantity  $\delta_A$  defined in (3) will play an important role in deriving our upper bound for  $\eta$ .*

### 2.2 THE UPPER BOUND FOR THE OVERLAP INDEX

We now proceed with deriving our proposed upper bound.

**Theorem 1.** *Without loss of generality, assume  $D^+$  and  $D^-$  are two probability distributions on a bounded domain  $B \subset \mathbb{R}^n$  with defined norm  $\|\cdot\|^1$  (i.e.,  $\sup_{x \in B} \|x\| < +\infty$ ), then for any subset*

<sup>1</sup>In this paper, we use the  $L_2$  norm. However, the choice of the norm is not unique and the analysis can be carried out using other norms as well.

---

$A \subset B$  with its complementary set  $A^c = B \setminus A$ , we have

$$\eta(D^+, D^-) \leq 1 - \frac{1}{2r_{A^c}} \|\mu_{D^+} - \mu_{D^-}\| - \frac{r_{A^c} - r_A}{r_{A^c}} \delta_A \quad (5)$$

where  $r_A = \sup_{x \in A} \|x\|$  and  $r_{A^c} = \sup_{x \in A^c} \|x\|$ ,  $\mu_{D^+}$  and  $\mu_{D^-}$  are the means of  $D^+$  and  $D^-$ , and  $\delta_A$  is the variation distance on set  $A$  defined in **Definition 3**. Moreover, let  $r_B = \sup_{x \in B} \|x\|$ , then we have

$$\eta(D^+, D^-) \leq 1 - \frac{1}{2r_B} \|\mu_{D^+} - \mu_{D^-}\| - \frac{r_B - r_A}{r_B} \delta_A. \quad (6)$$

Since (6) holds for any  $A$ , a tighter bound can be written as

$$\eta(D^+, D^-) \leq 1 - \frac{1}{2r_B} \|\mu_{D^+} - \mu_{D^-}\| - \max_A \frac{r_B - r_A}{r_B} \delta_A. \quad (7)$$

*Proof.* See Appendix A. □

**Remark 2.** The only assumption in this theorem is that the probability distribution domain is bounded. However, almost all real-world applications satisfy the boundedness assumption since the data is bounded. Therefore,  $r_B$  can always be found (or at least a reasonable approximation can be found). Additionally, we can constrain  $A$  to be a bounded ball so that  $r_A$  is also known. Although the proof of this theorem involves probability density functions, the computation does not require knowing the probability density functions but only finite samples because we can use the law of large numbers to estimate  $\|\mu_{D^+} - \mu_{D^-}\|$  and  $\delta_A$ , which will be shown next.

### 2.3 APPROXIMATING THE BOUND WITH FINITE SAMPLES

Let  $g : B \rightarrow \{0, 1\}$  be a condition function<sup>2</sup> and define  $A = \{x \mid g(x) = 1, x \in B\}$ . According to the definition of  $\delta_A$  and triangular inequality, it is trivial to prove that

$$\delta_A(D^+, D^-) \geq \frac{1}{2} |\mathbb{E}_{D^+}[g] - \mathbb{E}_{D^-}[g]|. \quad (8)$$

Calculating  $\mathbb{E}_{D^+}[g]$  and  $\mathbb{E}_{D^-}[g]$  is easy: one just needs to draw samples from  $D^+$  and  $D^-$ , and then average their  $g$  values. Applying (8) into **Theorem 1** gives the following corollary:

**Corollary 1.** Given  $D^+$ ,  $D^-$ ,  $B$ , and  $\|\cdot\|$  used in **Theorem 1**, let  $A(g) = \{x \mid g(x) = 1, x \in B\}$  with any condition function  $g : B \rightarrow \{0, 1\}$ . Then, an upper bound for  $\eta(D^+, D^-)$  that can be obtained by our approximation is

$$\eta(D^+, D^-) \leq 1 - \frac{1}{2r_B} \|\mu_{D^+} - \mu_{D^-}\| - \max_g \frac{r_B - r_{A(g)}}{2r_B} |\mathbb{E}_{D^+}[g] - \mathbb{E}_{D^-}[g]|. \quad (9)$$

Given several condition functions  $\{g_j\}_{j=1}^k$  and finite sample sets (i.e.,  $\{x_i^+\}_{i=1}^n \sim D^+$  and  $\{x_i^-\}_{i=1}^m \sim D^-$ ), Alg. 1 shows how to compute the RHS of (9).

---

**Algorithm 1** ComputeBound( $\{x_i^+\}_{i=1}^n, \{x_i^-\}_{i=1}^m, \{g_j\}_{j=1}^k$ )

---

```

 $B \leftarrow \{x_1^+, x_2^+, \dots, x_n^+, x_1^-, x_2^-, \dots, x_m^-\}$  and  $r_B \leftarrow \max_{x \in B} \|x\|$ 
 $\Delta_\mu \leftarrow \left\| \frac{1}{n} \sum_{i=1}^n x_i^+ - \frac{1}{m} \sum_{i=1}^m x_i^- \right\|$ 
for  $j = 1 \rightarrow k$  do
     $A = \{x \mid g_j(x) = 1, x \in B\}$  and  $r_A \leftarrow \max_{x \in A} \|x\|$ 
     $s_j \leftarrow \left(1 - \frac{r_A}{r_B}\right) \left| \frac{1}{n} \sum_{i=1}^n g_j(x_i^+) - \frac{1}{m} \sum_{i=1}^m g_j(x_i^-) \right|$ 
end for
Return:  $1 - \frac{1}{2r_B} \Delta_\mu - \frac{1}{2} \max_j s_j$ 

```

---

<sup>2</sup>The condition function is an indicator function  $\mathbb{1}\{condition\}$  that outputs 1 when the input satisfies the given condition and 0 otherwise.

---

**Remark 3.** The choice of condition functions is not unique. In this work, we use the indicator function  $g(x) = \mathbb{1}\{||x|| \leq r\}$ , which outputs 1 if  $||x|| \leq r$  and 0 otherwise. By setting different values for  $r$ , we generate a family of condition functions. The motivation for choosing such indicator function form is that it is the most simple way to separate a space nonlinearly and it saves computations by directly applying  $r$  into **Corollary 1**. However, other indicator functions, such as RBF kernel-based indicator functions, are worth exploring and will be considered in our future works.

### 3 APPLICATION OF OUR BOUND TO ONE-CLASS CLASSIFICATION

#### 3.1 PROBLEM FORMULATION FOR ONE-CLASS CLASSIFICATION

Given  $\mathbb{R}^d$  space and  $n$  samples  $\{x_i\}_{i=1}^n$  that lie in an unknown probability distribution, we would like to build a test  $\Psi : \mathbb{R}^d \rightarrow \{\pm 1\}$  so that for any new input  $x$ ,  $\Psi(x)$  outputs 1 when  $x$  is from the same unknown probability distribution, and outputs -1, otherwise. Some applications of  $\Psi$  are novelty detection, out-of-distribution detection, and backdoor detection (e.g., Fig. 1(b, c)).

#### 3.2 A NOVEL CONFIDENCE SCORE FUNCTION

Given some in-class samples  $\{x_i\}_{i=1}^n$ , one can pick several condition functions  $\{g_j\}_{j=1}^k$ , where  $g_j(x) = \mathbb{1}\{||x|| \leq r_j\}$  for different  $r_j$ , so that  $f(x) = \text{ComputeBound}(\{x\}, \{x_i\}_{i=1}^n, \{g_j\}_{j=1}^k)$  defined in Alg. 1 is a score function that measures the likelihood of any input,  $x$ , being an in-class sample. Alg. 2 shows the overall one-class classification algorithm.

---

**Algorithm 2** The Novel One-Class Classifier for the Input  $x$

---

```

Given in-class samples  $\{x_i\}_{i=1}^n$ , select several condition functions  $\{g_j\}_{j=1}^k$ , set a threshold  $T_0$ 
if  $\text{ComputeBound}(\{x\}, \{x_i\}_{i=1}^n, \{g_j\}_{j=1}^k) \geq T_0$  then
     $x$  is an in-class sample
else
     $x$  is an out-class sample
end if

```

---

**Remark 4.** The score function  $f$  measures the maximum similarity between the new input  $x$  and the available in-class samples  $\{x_i\}_{i=1}^n$ . Different  $T_0$  lead to different detection accuracy. However, we will show that the proposed one-class classifier has an overall high accuracy under different  $T_0$ .

#### 3.3 COMPUTATION AND SPACE COMPLEXITIES

Our algorithm can pre-compute and store  $\frac{1}{n} \sum_{i=1}^n x_i$  and  $\frac{1}{n} \sum_{i=1}^n g_j(x_i)$  with  $j = 1, 2, \dots, k$ . Therefore, the total space complexity is  $\mathcal{O}(k + 1)$ . Assume that the total number of new online inputs is  $l$ ; then, for every new input  $x$ , our algorithm needs to calculate  $||x||$  once and  $s_j$  for  $k$  times. Therefore, the total computation complexity is  $\mathcal{O}(l(k + 1))$ . Empirically, we restricted  $k$  to be a small number (e.g., 10) so that even devices without strong computation power can run our algorithm efficiently. Therefore, our classifier is computation-efficient and memory-efficient.

#### 3.4 EVALUATION

**Overall Setup:** We used  $r_j = \frac{j}{k} r_B$  with  $k = 50$  and  $r_B$  defined in **Theorem 1** unless specified. All the baseline algorithms with optimal hyperparameters, related datasets, and models were acquired from the corresponding authors' websites. The only exception is backdoor detection, in which we created our own models. However, we have carefully fine-tuned the baseline methods' hyperparameters to ensure their best performance over other hyperparameter choices.

##### 3.4.1 NOVELTY DETECTION

We evaluated our classifier on 100 small UCI datasets (UCI; Dua & Graff, 2017) and recorded the area under the receiver operating characteristic curve (AUROC). Fig. 2 shows the mean and standard

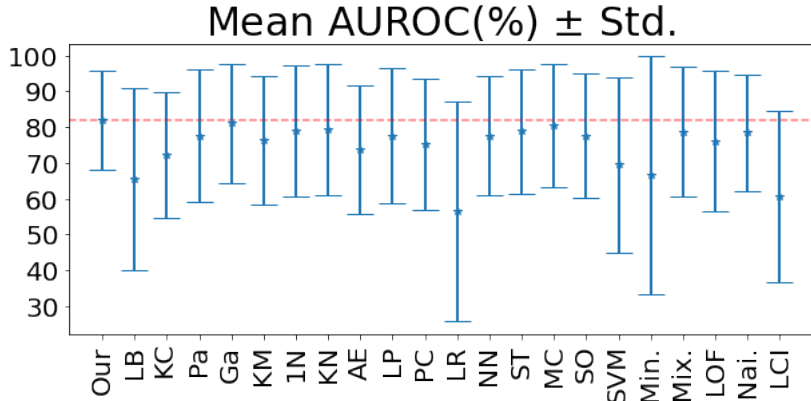


Figure 2: Evaluation on 100 small UCI datasets for novelty detection. Details are in Table 4.

Table 1: Average performance on various out-of-distribution datasets. Details are in Tables 5 and 6.

In-Distributions	Method	TPR95	AUROC	AUPR	Time/Sample	Memory
CIFAR-10	Ours	<b>81.39%</b>	<b>96.08%</b>	96.17%	3.0ms	<b>1048.22MiB</b>
	MSP	50.63%	91.46%	<b>98.07%</b>	<b>0.02ms</b>	1825.21MiB
	Mahala.	46.83%	90.46%	97.92%	30.61ms	1983.17MiB
	Energy	68.31%	92.32%	97.96%	0.22ms	1830.01MiB
	GEM	50.81%	90.45%	97.91%	25.62ms	1983.51MiB
CIFAR-100	Ours	<b>72.93%</b>	<b>93.53%</b>	93.69%	3.0ms	<b>1134.32MiB</b>
	MSP	19.87%	75.97%	94.09%	<b>0.02ms</b>	1825.98MiB
	Mahala.	48.35%	84.90%	96.37%	56.24ms	1983.81MiB
	Energy	27.91%	80.44%	95.15%	0.21ms	1838.23MiB
	GEM	48.36%	84.94%	<b>96.38%</b>	56.27ms	1984.77MiB

deviation of AUROC for ours and other classifiers. Detailed numerical results are in Table 4 in Appendix C. The implementation code is provided in the supplementary material.

Our classifier outperforms all the baseline methods by showing the highest average and lowest standard deviation of AUROC. Besides the results, our classifier is distribution-free, computation-efficient, and memory-efficient, whereas some other classifiers do not. Our method is also easy to explain and understand: the score measures the maximum similarity between the new input and the available in-class samples. Therefore, we conclude that our classifier is valid for novelty detection.

### 3.4.2 OUT-OF-DISTRIBUTION DETECTION

We used CIFAR-10 and CIFAR-100 testing datasets (Krizhevsky et al., 2009) as the in-distribution datasets. The compared methods contain MSP (Hendrycks & Gimpel, 2017), Mahalanobis (Lee et al., 2018), Energy score (Liu et al., 2020a), and GEM (Morteza & Li, 2022). We used WideResNet (Zagoruyko & Komodakis, 2016) to extract features from the raw data. The WideResNet models (well-trained on CIFAR-10 and CIFAR-100 training datasets) and corresponding feature extractors were acquired from Morteza & Li (2022). All the methods were evaluated in the same feature spaces with their optimal hyperparameters for fair comparisons. To fit the score function’s parameters for all the methods, we formed a small dataset by randomly selecting 10 samples from each class. The out-of-distribution datasets include Textures (Cimpoi et al., 2014), SVHN (Netzer et al., 2011), LSUN-Crop (Yu et al., 2015), LSUN-Resize (Yu et al., 2015), and iSUN (Xu et al., 2015). We used three metrics: the detection accuracy for out-of-distribution samples when the detection accuracy for in-distribution samples is 95% (TPR95), AUROC, and area under precision and recall (AUPR).

Table 1 shows the average results for CIFAR-10 and CIFAR-100. The details for each individual out-of-distribution dataset can be found in Tables 5 and 6 in Appendix D. Our method outperforms the other methods by using the least memory and showing the highest TPR95 and AUROC on average. The AUPR of our approach is in the same range as other baseline methods and the execution time of

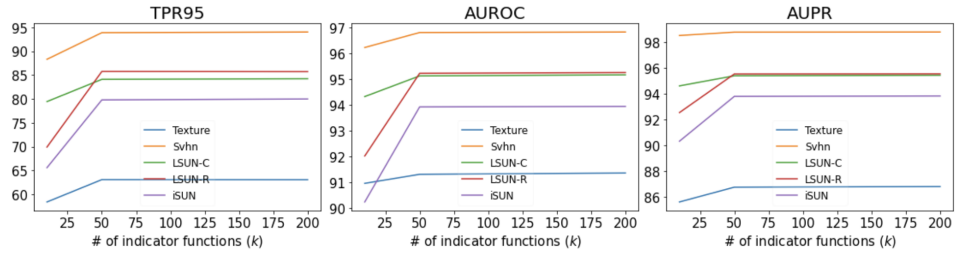


Figure 3: Performance of our approach with different  $k$  when CIFAR-10 is the in-distribution data.

Clean	Triggers			Clean	Triggers
<b>MNIST</b>	All label	Naive.1	Naive.2	<b>ImageNet</b>	<b>Invisible</b>
<b>CIFAR-10</b>	TCA.1	TCA.2	Wanet	<b>YouTube Face</b>	<b>Sunglasses</b>
<b>GTSRB</b>	Moving	Filter	Wanet		<b>Lipstick</b>

Figure 4: Pictures under "Triggers" are poisoned samples regarding different backdoored attacks. Pictures under "Clean" are clean samples for each dataset.

our approach for each sample is around 3 milliseconds (ms). We further evaluated our approach by using different numbers of indicator functions  $k$  and plotted the results in Fig. 3. From the figure, the performance of our approach increases with more indicator functions being used and eventually converges to a limit. This limit is determined by the out-of-distribution dataset, the tightness of our bound in **Corollary 1**, and the form of utilized indicator functions.

We also evaluated our approach with balanced datasets because the above out-of-distribution datasets are much different in size from the in-distribution datasets. On balanced datasets, our approach shows higher AUPR than the baseline methods as shown in Table 2 with details in Table 7 in Appendix E. We also empirically observed that the compared baseline methods reported errors when data dimensions are dependent because the compared baseline methods need to calculate the inverse of the estimated covariance matrices that will not be full rank if data dimensions are dependent. We have reported this observation in Table 7 in the appendix. In contrast, our approach works since it does not require finding the inverse of any matrices. Further, Table 1 and Table 2 together show that the baseline methods perform well only for out-of-distribution detection, whereas our approach performs well for both out-of-distribution detection and backdoor detection (details are explained in next subsection). In summary, our classifier is a valid out-of-distribution detector.

### 3.4.3 BACKDOOR DETECTION

The utilized datasets are MNIST (LeCun et al., 2010), CIFAR-10 (Krizhevsky et al., 2009), GTSRB (Stallkamp et al., 2011), YouTube Face (Wolf et al., 2011), and sub-ImageNet (Deng et al., 2009). The adopted backdoor attacks include naive triggers, all-label attacks (Gu et al., 2019), moving triggers (Fu et al., 2020), Wanet (Nguyen & Tran, 2021), combination attacks, large-sized triggers,

Table 2: Average performance for backdoor detection over various backdoor triggers and datasets.

Metrics (%)	Ours	STRIP	Mahalanobis	GEM	MSP
TPR95	89.40	39.60	56.97	<b>91.57</b>	39.24
AUROC	<b>96.68</b>	70.30	75.94	58.08	54.92
AUPR	<b>95.42</b>	68.76	76.37	75.88	60.52

Table 3: AUROC (%) on CIFAR-10 with different normal classes. **Boldface** shows the best performing algorithm, whereas underline shows the second best algorithm.

Methods	Air.	Aut.	Bird	Cat	Deer	Dog	Frog	Hor.	Ship	Tru.	Ave.
Ours	75.0	<b>67.9</b>	56.9	60.4	68.6	<u>63.1</u>	69.9	61.0	<u>77.9</u>	<b>76.0</b>	<b>67.7</b>
OCGAN	<b>75.7</b>	53.1	<b>64.0</b>	<b>62.0</b>	<b>72.3</b>	62.0	<b>72.3</b>	57.5	<b>82.0</b>	55.4	65.6
Deep SVDD	61.7	<u>65.9</u>	50.8	59.1	60.9	<b>65.7</b>	67.7	<b>67.3</b>	75.9	<u>73.1</u>	64.8
AnoGAN	67.1	54.7	52.9	54.5	65.1	60.3	58.5	<u>62.5</u>	75.8	66.5	61.8
DCAE	59.1	57.4	48.9	58.4	54.0	62.2	51.2	58.6	76.8	67.3	59.4

filter triggers, and invisible sample-specific triggers (Li et al., 2021), as listed in Fig. 4. The neural network architecture includes Network in Network (Lin et al., 2014), Resnet (He et al., 2016), and other networks from (Wang et al., 2019; Gu et al., 2019). For each backdoor attack, we assume that a small clean validation dataset is available (i.e., 10 samples from each class) at the beginning. Therefore, the poisoned samples (i.e., samples attached with triggers) can be considered out-class samples, whereas the clean samples can be considered in-class samples. We used the backdoored network to extract data features. Then, we evaluated our one-class classifier and compared it with the previous baseline methods and STRIP (Gao et al., 2019) in the feature space. The metrics used are the same: TPR95 (i.e., the detection accuracy for poisoned samples when the detection accuracy for clean samples is 95%), AUROC, and AUPR. Table 2 shows the average performance. Details on each individual trigger can be found in Table 7 in Appendix E

From the table, our classifier outperforms other baseline methods on average by showing the highest AUROC and AUPR. Additionally, our approach also has a very high TPR95. For each individual trigger, the TPR95 of our method is over 96% for most cases, the AUROC of our method is over 97% for most cases, and the AUPR of our method is over 95% for most cases. It is also seen that our classifier is robust against the latest or advanced backdoor attacks, such as Wanet, invisible trigger, all label attack, and filter attack, whereas the baseline methods show low performance on those attacks. Therefore, we conclude that our classifier is valid for backdoor detection.

#### 3.4.4 ANOMALY DETECTION WITH ITERATIVE SCORES

For an input  $x$ , denote the confidence score calculated using the condition functions  $g_j(x) = \mathbb{1}\{||x|| \leq r_j\}$  as  $s(x)$ , then its iterative confidence score,  $s'(x)$ , is calculated by Alg. 1 but with the new condition functions  $g'_j(x) = \mathbb{1}\{s(x) \leq \frac{j}{k}\}$ . To evaluate the efficacy of this iterative approach, we consider the comparison with deep network-based classifiers, including DCAE (Makhzani & Frey, 2015), AnoGAN (Schlegl et al., 2017), Deep SVDD (Ruff et al., 2018), and OCGAN (Perea et al., 2019), for anomaly detection on the CIFAR-10 dataset in the raw image space. The anomaly detection setting considers one class as normal and the remaining classes as anomalous. The baseline methods need to first train deep networks on available normal-class samples and then use the trained models to detect anomalies, whereas our approach does not require this training process. Additionally, we empirically observed that the baseline methods require around 5000 available normal-class training samples to be effective, whereas our approach needs only 100 available normal samples to be effective. For a fair comparison, we allow the baseline methods to use 5000 available normal-class samples to train their deep networks to achieve their best performance.

Table 3 shows the results. Our approach shows the highest AUROC on average. Additionally, our approach shows either the best or the second-best performance for 9 individual cases. Moreover, if the baseline methods are trained with only 100 available normal samples, then their performance will become lower. For example, Deep SVDD shows only 61.1% AUROC on average. Therefore, our approach is valid and sample-efficient in the raw image space and outperforms the deep network-based anomaly detection methods.

## 4 APPLICATION OF OUR BOUND TO DOMAIN SHIFT ANALYSIS

Our bound is also useful in domain shift analysis.

**Theorem 2.** *Assume that  $D$  and  $D^*$  are two different data distributions (i.e.,  $\eta(D, D^*) < 1$ ) and denote the overall accuracy of the model on  $D^*$  as  $Acc$ . If a model is trained on  $D$  with  $p$  accuracy on  $D$  and  $q$  accuracy on  $D^* \setminus D$ , then we have*

$$Acc \leq (p - q)(1 - \frac{1}{2r_B} \|\mu_D - \mu_{D^*}\|) - \max_g \frac{r_B - r_{A(g)}}{2r_B} |\mathbb{E}_D[g] - \mathbb{E}_{D^*}[g]| + q. \quad (10)$$

*Proof.* See Appendix B.  $\square$

**Remark 5.** *As one case of the domain shift, a backdoor attack scenario (Fig. 1(b)) considers that the model has a zero accuracy on poisoned data distribution (i.e.,  $q = 0$ ) as the attack success rate is almost 100%. Define the clean data distribution as  $D$ , poisoned data distribution as  $D^p$ , and a testing data distribution  $D^*$  composed by  $D$  and  $D^p$ , i.e.,  $D^* = \sigma D + (1 - \sigma)D^p$ , where  $\sigma \in [0, 1]$  is the purity ratio (i.e., the ratio of clean samples to the entire testing samples). Then (10) becomes*

$$Acc \leq p(1 - \frac{1 - \sigma}{2r_B} \|\mu_D - \mu_{D^p}\|) - (1 - \sigma) \max_g \frac{r_B - r_{A(g)}}{2r_B} |\mathbb{E}_D[g] - \mathbb{E}_{D^p}[g]|. \quad (11)$$

**Experimental Illustration of Theorem 2:** The backdoor attack scenario is used to illustrate Theorem 2 using MNIST, GTSRB, YouTube Face, and sub-ImageNet datasets and their domain-shifted versions shown in ‘‘All label’’ for MNIST, ‘‘Filter’’ for GTSRB, ‘‘Sunglasses’’ for YouTube Face, and ‘‘Invisible’’ for sub-ImageNet in Fig. 4. We composed the testing datasets  $D^*$  with  $\sigma = 0, 0.1, \dots, 0.9, 1$  and calculated the RHS of (11) using  $L_1$ ,  $L_2$ , and  $L_\infty$  norms in the raw image space, model output space, and hidden layer space. Fig. 5 shows the actual model accuracy and corresponding upper bounds with different  $\sigma$ s. The actual model accuracy is below all the calculated upper limits, which validates **Theorem 2**.

Additionally, the difference between actual model accuracy and the calculated upper bound accuracy can reflect the extent of the domain shift in the test dataset. From Fig. 5, a large difference reflects a large domain shift. When the domain shift vanishes, the actual model accuracy and the calculated upper bound accuracy coincide. Compared to other methods, our approach is time-efficient.

**Theorem 2** can also help infer useful data information to most likely find and remove domain-shifted samples to eliminate the domain shift. Specifically, from Fig. 5, the calculated upper bound accuracy varies with norms and feature spaces. The inference is that a low calculated upper bound accuracy implies a high likelihood of distinguishing original and domain-shifted data distributions in that particular utilized feature space. For example, in Fig. 5 MNIST and YouTube, the input space with  $L_\infty$  norm shows the lowest calculated upper bound accuracy. Therefore, the inference is that the original and domain-shifted data distributions are likely to be distinguished in the raw image space. Indeed, even vision inspection can easily distinguish original and domain-shifted samples for the MNIST and YouTube cases given their domain-shifted samples under ‘‘All label’’ and ‘‘Sunglasses’’ in Fig. 4. As for GTSRB and ImageNet, the input space has the highest upper limit lines. Therefore, the original and domain-shifted data distributions are less likely to be distinguished in the raw image space. Since their domain-shifted samples are ‘‘Filter’’ and ‘‘Invisible’’ in Fig. 4, the vision inspection barely discriminates between original and domain-shifted samples for GTSRB and sub-ImageNet. Moreover, the hidden layer space gives the lowest estimated upper bound accuracy for GTSRB and ImageNet. Therefore, original and domain-shifted samples are more likely to be visually distinguished in the hidden layer space as shown in Fig. 6.

## 5 CONCLUSION

This paper proposes an easy-to-compute distribution-free upper bound for the distribution overlap index. The computation of the bound is time-efficient and memory-efficient and only requires finite samples. Two applications of the bound are explored. The first application is for one-class classification. Specifically, this paper introduces a novel distribution-free one-class classifier with the bound being its confidence score function. The classifier is sample-efficient, computation-efficient, and memory-efficient. The proposed classifier is evaluated on novelty detection, out-of-distribution

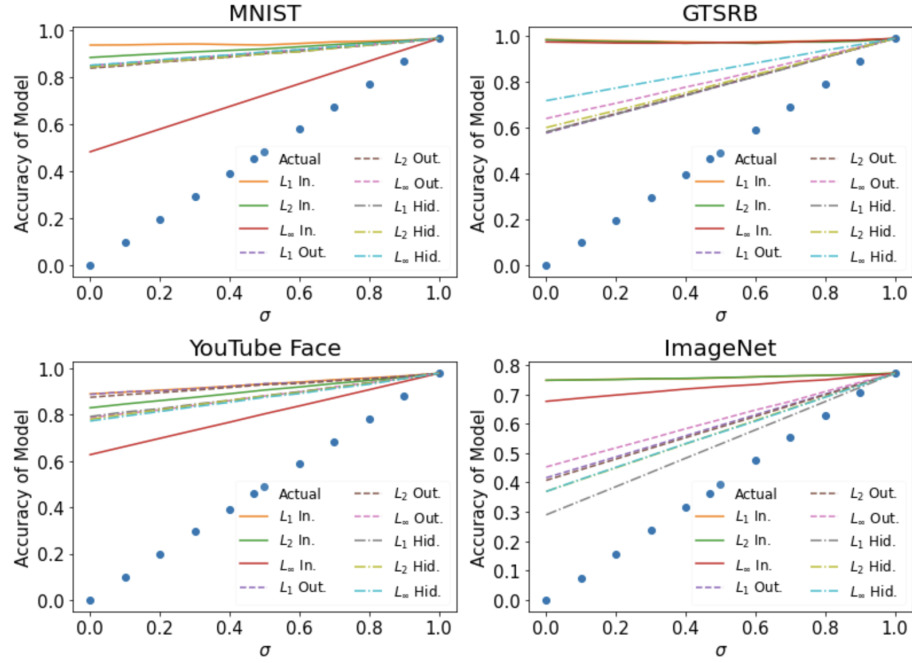


Figure 5: The actual model accuracy (dot) vs. (10) (solid) calculated with  $L_1$ ,  $L_2$ , and  $L_\infty$  norms in input, output, and hidden spaces. x: the ratio of clean samples to the entire testing samples.

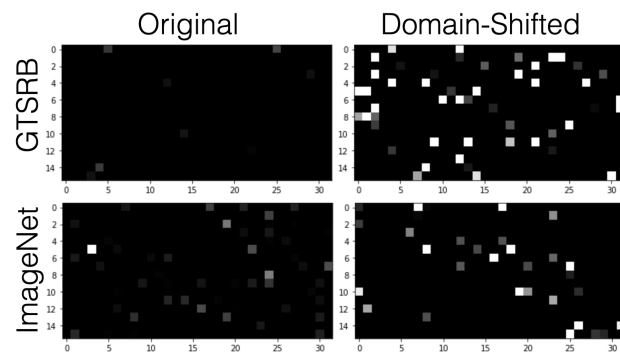


Figure 6: Original and domain-shifted sample in the hidden layer space.

---

detection, backdoor detection, and anomaly detection on various datasets and outperforms many state-of-the-art methods. The second application is for domain shift analysis with a proposed theorem to detect the domain shift existence and infer useful data information. The obtained results show significant promise toward broadening the application of overlap-based metrics.

---

## REFERENCES

- One-class classifier results. <http://homepage.tudelft.nl/n9d04/occ/index.html>. Accessed: 2022-08-30.
- Anil Bhattacharyya. On a measure of divergence between two statistical populations defined by their probability distributions. *Bulletin of the Calcutta Mathematical Society*, 35:99–109, 1943.
- Battista Biggio, Blaine Nelson, and Pavel Laskov. Poisoning attacks against support vector machines. In *Proceedings of the International Conference on International Conference on Machine Learning*, pp. 1467–1474, Edinburgh, Scotland, June 2012.
- Mircea Cimpoi, Subhransu Maji, Iasonas Kokkinos, Sammy Mohamed, and Andrea Vedaldi. Describing textures in the wild. In *Proceedings of the IEEE Conference on Computer Vision and Pattern Recognition*, pp. 3606–3613, Columbus, OH, June 2014.
- Jacob Cohen. *Statistical power analysis for the behavioral sciences*. Routledge, 2013.
- Francesco De Comité, François Denis, Rémi Gilleron, and Fabien Letouzey. Positive and unlabeled examples help learning. In *Proceedings of International Conference on Algorithmic Learning Theory*, pp. 219–230, Tokyo, Japan, Dec. 1999.
- J. Deng, W. Dong, R. Socher, L. Li, Kai Li, and Li Fei-Fei. Imagenet: A large-scale hierarchical image database. In *Proceedings of the IEEE Conference on Computer Vision and Pattern Recognition*, pp. 248–255, Miami, FL, 2009.
- Dheeru Dua and Casey Graff. UCI machine learning repository, 2017. URL <http://archive.ics.uci.edu/ml>.
- Hao Fu, Akshaj Kumar Veldanda, Prashanth Krishnamurthy, Siddharth Garg, and Farshad Khorrami. Detecting backdoors in neural networks using novel feature-based anomaly detection. *arXiv preprint arXiv:2011.02526*, 2020.
- Hao Fu, Akshaj Kumar Veldanda, Prashanth Krishnamurthy, Siddharth Garg, and Farshad Khorrami. A feature-based on-line detector to remove adversarial-backdoors by iterative demarcation. *IEEE Access*, 10:5545 – 5558, 2022.
- Yansong Gao, Change Xu, Derui Wang, Shiping Chen, Damith C Ranasinghe, and Surya Nepal. Strip: A defence against trojan attacks on deep neural networks. In *Proceedings of the Annual Computer Security Applications Conference*, pp. 113–125, Austin, TX, Dec. 2019.
- C Gini and G Livada. Nuovi contributi alla teoria della transvariazione. *Roma: Atti della VI Riunione della Società Italiana di Statistica*, 1943.
- Ian Goodfellow, Jean Pouget-Abadie, Mehdi Mirza, Bing Xu, David Warde-Farley, Sherjil Ozair, Aaron Courville, and Yoshua Bengio. Generative adversarial nets. In *Proceedings of Advances in Neural Information Processing Systems*, volume 27, Montreal, Canada, Dec. 2014.
- Tianyu Gu, Kang Liu, Brendan Dolan-Gavitt, and Siddharth Garg. Badnets: Evaluating backdooring attacks on deep neural networks. *IEEE Access*, 7:47230–47244, 2019.
- Kaiming He, Xiangyu Zhang, Shaoqing Ren, and Jian Sun. Deep residual learning for image recognition. In *Proceedings of the IEEE Conference on Computer Vision and Pattern Recognition*, pp. 770–778, Miami, FL, June 2016.
- Ernst Hellinger. Neue begründung der theorie quadratischer formen von unendlichvielen veränderlichen. *Journal für die reine und angewandte Mathematik*, 1909(136):210–271, 1909.
- Dan Hendrycks and Kevin Gimpel. A baseline for detecting misclassified and out-of-distribution examples in neural networks. In *Proceedings of International Conference on Learning Representations*, Toulon, France, Apr. 2017.
- Carl J Huberty and Laureen L Lowman. Group overlap as a basis for effect size. *Educational and Psychological Measurement*, 60(4):543–563, 2000.

- 
- Shehroz S Khan and Michael G Madden. One-class classification: taxonomy of study and review of techniques. *The Knowledge Engineering Review*, 29(3):345–374, 2014.
- Alex Krizhevsky, Geoffrey Hinton, et al. Learning multiple layers of features from tiny images, 2009.
- Solomon Kullback and Richard A Leibler. On information and sufficiency. *The Annals of Mathematical Statistics*, 22(1):79–86, 1951.
- Yann LeCun, Corinna Cortes, and CJ Burges. Mnist handwritten digit database. *ATT Labs [Online]*. Available: <http://yann.lecun.com/exdb/mnist>, 2, 2010.
- Kimin Lee, Kibok Lee, Honglak Lee, and Jinwoo Shin. A simple unified framework for detecting out-of-distribution samples and adversarial attacks. In *Proceedings of Advances in Neural Information Processing Systems*, volume 31, Montreal, Canada, Dec. 2018.
- Yuezun Li, Yiming Li, Baoyuan Wu, Longkang Li, Ran He, and Siwei Lyu. Invisible backdoor attack with sample-specific triggers. In *Proceedings of the IEEE/CVF International Conference on Computer Vision*, pp. 16463–16472, Virtual, June 2021.
- Min Lin, Qiang Chen, and Shuicheng Yan. Network in network. In *Proceedings of the International Conference on Learning Representations*, pp. 1–10, Banff, Canada, Apr. 2014.
- Kang Liu, Brendan Dolan-Gavitt, and Siddharth Garg. Fine-pruning: Defending against backdooring attacks on deep neural networks. In *Proceedings of International Symposium on Research in Attacks, Intrusions, and Defenses*, pp. 273–294, Crete, Greece, Sep. 2018a.
- Weitang Liu, Xiaoyun Wang, John Owens, and Yixuan Li. Energy-based out-of-distribution detection. In *Proceedings of Advances in Neural Information Processing Systems*, volume 33, pp. 21464–21475, Virtual, Dec. 2020a.
- Yingqi Liu, Shiqing Ma, Yousra Aafer, Wen-Chuan Lee, Juan Zhai, Weihang Wang, and Xiangyu Zhang. Trojaning attack on neural networks. In *Proceedings of the Network and Distributed Systems Security Symposium*, San Diego, CA, Feb. 2018b.
- Yunfei Liu, Xingjun Ma, James Bailey, and Feng Lu. Reflection backdoor: A natural backdoor attack on deep neural networks. In *Proceedings of the European Conference on Computer Vision*, pp. 182–199, Virtual, Aug. 2020b.
- Alireza Makhzani and Brendan J Frey. Winner-take-all autoencoders. In C. Cortes, N. Lawrence, D. Lee, M. Sugiyama, and R. Garnett (eds.), *Advances in Neural Information Processing Systems*, volume 28, pp. 2791–2799, Montréal, Canada, Dec. 2015.
- Kenneth O McGraw and Seok P Wong. A common language effect size statistic. *Psychological Bulletin*, 111(2):361, 1992.
- Peyman Morteza and Yixuan Li. Provable guarantees for understanding out-of-distribution detection. In *Proceedings of the AAAI Conference on Artificial Intelligence*, volume 8, Virtual, Feb. 2022.
- Mary M Moya and Don R Hush. Network constraints and multi-objective optimization for one-class classification. *Neural Networks*, 9(3):463–474, 1996.
- Yuval Netzer, Tao Wang, Adam Coates, Alessandro Bissacco, Bo Wu, and Andrew Y Ng. Reading digits in natural images with unsupervised feature learning. In *Proceedings of NIPS Workshop on Deep Learning and Unsupervised Feature Learning*, Granada, Spain, Dec. 2011.
- Tuan Anh Nguyen and Anh Tuan Tran. Wanet - imperceptible warping-based backdoor attack. In *Proceedings of the International Conference on Learning Representations*, Virtual, May 2021.
- Massimiliano Pastore and Antonio Calcagnì. Measuring distribution similarities between samples: A distribution-free overlapping index. *Frontiers in Psychology*, 10:1089, 2019.

- 
- Pramuditha Perera, Ramesh Nallapati, and Bing Xiang. Ocgan: One-class novelty detection using gans with constrained latent representations. In *Proceedings of the IEEE/CVF Conference on Computer Vision and Pattern Recognition*, pp. 2898–2906, Long Beach, CA, June 2019.
- Lukas Ruff, Robert Vandermeulen, Nico Goernitz, Lucas Deecke, Shoaib Ahmed Siddiqui, Alexander Binder, Emmanuel Müller, and Marius Kloft. Deep one-class classification. In *Proceedings of International Conference on Machine Learning*, pp. 4393–4402, Stockholm , Sweden, July 2018.
- Thomas Schlegl, Philipp Seeböck, Sebastian M Waldstein, Ursula Schmidt-Erfurth, and Georg Langs. Unsupervised anomaly detection with generative adversarial networks to guide marker discovery. In *International Conference on Information Processing in Medical Imaging*, pp. 146–157. Springer, 2017.
- Bernhard Schölkopf, John C Platt, John Shawe-Taylor, Alex J Smola, and Robert C Williamson. Estimating the support of a high-dimensional distribution. *Neural Computation*, 13(7):1443–1471, 2001.
- Johannes Stallkamp, Marc Schlipsing, Jan Salmen, and Christian Igel. The german traffic sign recognition benchmark: A multi-class classification competition. In *Proceedings of the International Joint Conference on Neural Networks*, pp. 1453–1460, San Jose, CA, July 2011.
- David Martinus Johannes Tax. *One-class classification: Concept learning in the absence of counter-examples*. PhD thesis, Technische Universiteit Delft, 2002.
- Akshaj Kumar Veldanda, Kang Liu, Benjamin Tan, Prashanth Krishnamurthy, Farshad Khorrami, Ramesh Karri, Brendan Dolan-Gavitt, and Siddharth Garg. Nnociation: Catching badnets in the wild. In *Proceedings of the ACM Workshop on Artificial Intelligence and Security*, pp. 49–60, Virtual, Nov. 2021.
- Bolun Wang, Yuanshun Yao, Shawn Shan, Huiying Li, Bimal Viswanath, Haitao Zheng, and Ben Y Zhao. Neural cleanse: Identifying and mitigating backdoor attacks in neural networks. In *Proceedings of IEEE Symposium on Security and Privacy*, pp. 707–723, San Francisco, CA, May 2019.
- Murray S Weitzman. *Measures of overlap of income distributions of white and Negro families in the United States*, volume 3. US Bureau of the Census, 1970.
- Lior Wolf, Tal Hassner, and Itay Maoz. Face recognition in unconstrained videos with matched background similarity. In *Proceedings of the IEEE Conference on Computer Vision and Pattern Recognition*, pp. 529–534, Colorado Springs, CO, June 2011.
- Pingmei Xu, Krista A Ehinger, Yinda Zhang, Adam Finkelstein, Sanjeev R Kulkarni, and Jianxiong Xiao. Turker gaze: Crowdsourcing saliency with webcam based eye tracking. *arXiv preprint arXiv:1504.06755*, 2015.
- Jingkang Yang, Kaiyang Zhou, Yixuan Li, and Ziwei Liu. Generalized out-of-distribution detection: A survey. *arXiv preprint arXiv:2110.11334*, 2021.
- Fisher Yu, Ari Seff, Yinda Zhang, Shuran Song, Thomas Funkhouser, and Jianxiong Xiao. Lsun: Construction of a large-scale image dataset using deep learning with humans in the loop. *arXiv preprint arXiv:1506.03365*, 2015.
- Sergey Zagoruyko and Nikos Komodakis. Wide residual networks. *arXiv preprint arXiv:1605.07146*, 2016.
- Yi Zeng, Won Park, Z Morley Mao, and Ruoxi Jia. Rethinking the backdoor attacks’ triggers: A frequency perspective. In *Proceedings of the IEEE/CVF International Conference on Computer Vision*, pp. 16473–16481, 2021.

## A PROOF OF Theorem 1

*Proof.* Let  $f_{D^+}$  and  $f_{D^-}$  be the probability density functions for  $D^+$  and  $D^-$ . From (4), we have

$$\eta(D^+, D^-) = 1 - \delta_A(D^+, D^-) - \delta_{A^c}(D^+, D^-). \quad (12)$$

Using (12), triangular inequality, and boundedness, we obtain

$$\|\mu_{D^+} - \mu_{D^-}\| = \left\| \int_B x (f_{D^+}(x) - f_{D^-}(x)) dx \right\| \leq \int_B \|x(f_{D^+}(x) - f_{D^-}(x))\| dx \quad (13)$$

$$= \int_A \|x\| \cdot |f_{D^+}(x) - f_{D^-}(x)| dx + \int_{A^c} \|x\| \cdot |f_{D^+}(x) - f_{D^-}(x)| dx \quad (14)$$

$$\leq 2r_A \delta_A + 2r_{A^c} \delta_{A^c} = 2r_A \delta_A + 2r_{A^c} (1 - \delta_A - \eta(D^+, D^-)) \quad (15)$$

which implies (5). Replacing  $r_{A^c}$  with  $r_B$  in (15) implies (6).  $\square$

## B PROOF OF Theorem 2

*Proof.* Let  $f_D$  and  $f_{D^*}$  be their probability density functions, then

$$Acc = \int_{x \sim D^*} \left( p \frac{\min\{f_D(x), f_{D^*}(x)\}}{f_{D^*}(x)} + q \left( 1 - \frac{\min\{f_D(x), f_{D^*}(x)\}}{f_{D^*}(x)} \right) \right) f_{D^*}(x) dx \quad (16)$$

$$= p\eta(D, D^*) + q(1 - \eta(D, D^*)) = (p - q)\eta(D, D^*) + q \quad (17)$$

$$\leq (p - q)\left(1 - \frac{1}{2r_B}\|\mu_D - \mu_{D^*}\|\right) - \max_g \frac{r_B - r_{A(g)}}{2r_B} |\mathbb{E}_D[g] - \mathbb{E}_{D^*}[g]| + q. \quad (18)$$

$\square$

## C DETAILS FOR NOVELTY DETECTION

The method in Table 4 is in the same order as shown in Fig. 2.

Table 4: Means and standard deviations of AUROC (%) for different methods on 100 UCI datasets.

Ours	L1-Ball	K-Center	Parzen	Gaussian	K-Mean
$81.9 \pm 13.8$	$65.4 \pm 25.4$	$72.2 \pm 17.6$	$77.6 \pm 18.6$	$81.1 \pm 16.6$	$76.3 \pm 17.9$
1-Nearest Neighbor	K-Nearest Neighbor	Auto-Encoder Network	Linear Programming	Principal Component	Lof Range
$78.8 \pm 18.3$	$79.2 \pm 18.3$	$73.7 \pm 17.9$	$77.5 \pm 18.9$	$75.1 \pm 18.3$	$56.5 \pm 30.8$
Nearest Neighbor Distance	Minimum Spanning Tree	Minimum Covariance Determinant	Self Organizing Map	Support Vector Machine	Minimax Probability Machine
$77.5 \pm 16.6$	$78.8 \pm 17.4$	$80.4 \pm 17.1$	$77.6 \pm 17.4$	$69.4 \pm 24.6$	$66.4 \pm 33.3$
Mixture Gaussians	Local Outlier Factor	Naive Parzen	Local Correlation Integral		
$78.7 \pm 18.1$	$76.1 \pm 19.7$	$78.4 \pm 16.2$	$60.7 \pm 23.9$		

## D DETAILS FOR OUT-OF-DISTRIBUTION DETECTION

Table 5 is for CIFAR-10 case and Table 6 is for CIFAR-100 case.

## E DETAILS FOR BACKDOOR DETECTION

Table 7 shows the details for backdoor detection.

Table 5: Results for CIFAR-10 in-distribution case (higher number implies higher accuracy). **Bold-face** shows the best performing algorithm, whereas underline shows the second best algorithm.

Out-of-Distribution Datasets	Method	TPR95 (%)	AUROC (%)	AUPR (%)
Texture	Ours	<u>64.20</u>	92.80	92.33
	MSP	<u>40.75</u>	88.31	97.08
	Mahalanobis	62.38	<u>94.46</u>	<u>98.75</u>
	Energy Score	47.47	85.47	95.58
	GEM	<b>72.61</b>	<b>94.59</b>	<b>98.79</b>
SVHN	Ours	<b>94.10</b>	<b>98.56</b>	<b>99.41</b>
	MSP	52.41	92.11	98.32
	Mahalanobis	<u>79.34</u>	<u>95.72</u>	<u>99.04</u>
	Energy Score	64.20	91.05	97.66
	GEM	79	95.65	99.01
LSUN-Crop	Ours	<u>83.63</u>	<u>96.60</u>	96.61
	MSP	<u>69.07</u>	<u>95.64</u>	<u>99.13</u>
	Mahalanobis	30.06	86.15	97.05
	Energy Score	<b>91.89</b>	<b>98.40</b>	<b>99.67</b>
	GEM	30.20	86.09	97.03
LSUN-Resize	Ours	<b>85.41</b>	<b>96.84</b>	96.86
	MSP	47.45	91.30	<u>98.11</u>
	Mahalanobis	35.64	88.12	97.45
	Energy Score	<u>71.75</u>	<u>94.12</u>	<b>98.64</b>
	GEM	35.45	88.09	97.43
iSUN	Ours	<b>79.62</b>	<b>95.64</b>	95.68
	MSP	43.40	89.72	<u>97.72</u>
	Mahalanobis	26.77	87.87	97.33
	Energy Score	<u>66.27</u>	<u>92.56</u>	<b>98.25</b>
	GEM	36.80	87.85	93.33
Average Performance	Ours	<b>81.39</b>	<b>96.08</b>	96.17
	MSP	50.63	91.46	<b>98.07</b>
	Mahalanobis	46.83	90.46	97.92
	Energy Score	<u>68.31</u>	<u>92.32</u>	<u>97.96</u>
	GEM	50.81	90.45	97.91

Table 6: Results for CIFAR-100 in-distribution case (higher number implies higher accuracy). **Bold-face** shows the best performing algorithm, whereas underline shows the second best algorithm.

Out-of-Distribution Datasets	Method	TPR95 (%)	AUROC (%)	AUPR (%)
Texture	Ours	42.50	85.79	85.27
	MSP	16.71	73.58	93.02
	Mahalanobis	<b>57.62</b>	<u>90.14</u>	<u>97.62</u>
	Energy Score	20.38	76.46	93.68
	GEM	<u>57.40</u>	<b>90.17</b>	<b>97.63</b>
SVHN	Ours	<b>93.75</b>	<b>98.36</b>	<b>99.36</b>
	MSP	15.66	71.37	92.89
	Mahalanobis	51.35	89.25	97.52
	Energy Score	14.59	74.10	93.65
	GEM	<u>51.51</u>	<u>89.40</u>	<u>97.57</u>
LSUN-Crop	Ours	<u>57.76</u>	<u>89.95</u>	90.03
	MSP	<u>33.44</u>	83.71	<u>96.32</u>
	Mahalanobis	1.53	58.48	89.73
	Energy Score	<b>64.01</b>	<b>93.41</b>	<b>98.59</b>
	GEM	1.70	58.42	89.70
LSUN-Resize	Ours	<b>88.49</b>	<b>97.56</b>	97.55
	MSP	16.54	75.32	94.03
	Mahalanobis	<u>67.20</u>	93.97	<b>98.70</b>
	Energy Score	21.38	79.29	94.97
	GEM	67.09	<u>94.01</u>	<b>98.70</b>
iSUN	Ours	<b>82.15</b>	<b>96.05</b>	96.24
	MSP	17.02	75.87	94.20
	Mahalanobis	64.07	92.69	<b>98.32</b>
	Energy Score	19.20	78.98	94.90
	GEM	<u>64.10</u>	<u>92.73</u>	<b>98.32</b>
Average Performance	Ours	<b>72.93</b>	<b>93.53</b>	93.69
	MSP	19.87	75.97	94.09
	Mahalanobis	48.35	84.90	<u>96.37</u>
	Energy Score	27.91	80.44	95.15
	GEM	<u>48.36</u>	<u>84.94</u>	<b>96.38</b>

Table 7: Comparison results for backdoor detection (higher number implies higher accuracy).

Datasets	Trigger	Metrics (%)	Ours	STRIP	Mahalanobis	GEM	MSP	
MNIST	All label	TPR95	83.05	2.58	50.83	<b>100</b>	100	
		AUROC	<b>96.13</b>	44.69	90.78	50.43	50	
		AUPR	<b>94.20</b>	35.47	86.71	70.94	70.83	
MNIST	Naive.1	TPR95	<b>100</b>	98.85	99.86	100	5.11	
		AUROC	<b>97.50</b>	97.32	97.49	53.95	51.64	
		AUPR	96.17	95.95	<b>96.38</b>	74.74	50.41	
MNIST	Naive.2	TPR95	96.53	67.46	35.16	<b>100</b>	14.69	
		AUROC	<b>97.28</b>	93.67	78.63	53.51	58.14	
		AUPR	<b>95.75</b>	89.85	78.65	74.62	64.16	
CIFAR-10	TCA.1	TPR95	<b>100</b>	35.68	100	100	4.38	
		AUROC	<b>97.50</b>	83.00	97.49	50	49.23	
		AUPR	95.47	73.22	<b>97.84</b>	76.32	52.64	
CIFAR-10	TCA.2	TPR95	<b>100</b>	27.86	100	100	0.02	
		AUROC	<b>97.50</b>	68.79	97.49	50	29.90	
		AUPR	<b>97.63</b>	72.41	95.86	67.86	18.05	
CIFAR-10	Wanet	TPR95	37.87	0.07	20.35	22.90	<b>100</b>	
		AUROC	<b>92.74</b>	34.97	50.61	57.81	50	
		AUPR	<b>89.95</b>	37.42	57.30	68.48	74.87	
GTSRB	Moving	TPR95	<b>99.99</b>	54				
		AUROC	<b>85.39</b>	7.29	Fail: dependent data dimensions			
		AUPR	<b>96.96</b>	89.07				
GTSRB	Filter	TPR95	<b>85.39</b>	7.29				
		AUROC	<b>96.54</b>	38.92	Fail: dependent data dimensions			
		AUPR	<b>95.42</b>	38.81				
GTSRB	Wanet	TPR95	<b>100</b>	1.24	0.51	100	100	
		AUROC	<b>97.50</b>	36.31	54.46	50	50	
		AUPR	<b>97.62</b>	39.53	48.92	75.23	75.23	
YouTube Face	Sunglasses	TPR95	73.37	83.03	71.64	<b>98.58</b>	13.06	
		AUROC	<b>95.21</b>	94.80	94.38	84.29	66.55	
		AUPR	93.00	<b>95.54</b>	94.63	88.83	53.27	
YouTube Face	Lipstick	TPR95	<b>96.64</b>	90.14	90.88	94.18	3.73	
		AUROC	<b>97.21</b>	93.15	93.26	80.80	50.14	
		AUPR	<b>96.30</b>	94.98	95.09	86.53	53.27	
sub-ImageNet	Invisible	TPR95	<b>100</b>	7.01	0.5	100	51.40	
		AUROC	<b>97.49</b>	66.26	4.78	50	93.61	
		AUPR	<b>96.53</b>	62.83	12.27	75.26	92.46	
Average Performance		TPR95	89.40	39.60	56.97	<b>91.57</b>	39.24	
		AUROC	<b>96.68</b>	70.30	75.94	58.08	54.92	
		AUPR	<b>95.42</b>	68.76	76.37	75.88	60.52	